

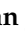



Article

Improved Procedure for Multi-Focus Images Using Image Fusion with qshiftN DTCWT and MPCA in Laplacian Pyramid Domain

Chinnem Rama Mohan ¹, Kuldeep Chouhan ², Ranjeet Kumar Rout ³, Kshira Sagar Sahoo ⁴,
Noor Zaman Jhanjhi ^{5,*}, Ashraf Osman Ibrahim ⁶ and Abdelzahir Abdelmaboud ⁷

¹ Department of Computer Science and Engineering, Visvesvaraya Technological University, Belgaum 590018, India

² Department of Computer Science and Engineering, Shivalik College of Engineering, Dehradun 248197, India

³ Computer Science and Engineering, National Institute of Technology Srinagar, Srinagar 190006, India

⁴ Department of Computer Science and Engineering, SRM University, Amaravati 522240, India

⁵ School of Computer Science and Engineering, Taylor's University, Subang Jaya 47500, Malaysia

⁶ Faculty of Computing and Informatics, University Malaysia Sabah, Kota Kinabalu 88400, Malaysia

⁷ Department of Information Systems, King Khalid University, Muhayil Asir 61913, Saudi Arabia

* Correspondence: noorzaman.jhanjhi@taylor.edu.my

Abstract: Multi-focus image fusion (MIF) uses fusion rules to combine two or more images of the same scene with various focus values into a fully focused image. An all-in-focus image refers to a fully focused image that is more informative and useful for visual perception. A fused image with high quality is essential for maintaining shift-invariant and directional selectivity characteristics of the image. Traditional wavelet-based fusion methods, in turn, create ringing distortions in the fused image due to a lack of directional selectivity and shift-invariance. In this paper, a classical MIF system based on quarter shift dual-tree complex wavelet transform (qshiftN DTCWT) and modified principal component analysis (MPCA) in the laplacian pyramid (LP) domain is proposed to extract the focused image from multiple source images. In the proposed fusion approach, the LP first decomposes the multi-focus source images into low-frequency (LF) components and high-frequency (HF) components. Then, qshiftN DTCWT is used to fuse low and high-frequency components to produce a fused image. Finally, to improve the effectiveness of the qshiftN DTCWT and LP-based method, the MPCA algorithm is utilized to generate an all-in-focus image. Due to its directionality, and its shift-invariance, this transform can provide high-quality information in a fused image. Experimental results demonstrate that the proposed method outperforms many state-of-the-art techniques in terms of visual and quantitative evaluations.

Keywords: image quality; quarter shift dual-tree complex wavelet transform; laplacian pyramid; modified principal component analysis; multi-focus image fusion; quality evaluation metrics



Citation: Mohan, C.R.; Chouhan, K.; Rout, R.K.; Sahoo, K.S.; Jhanjhi, N.Z.; Ibrahim, A.O.; Abdelmaboud, A. Improved Procedure for Multi-Focus Images Using Image Fusion with qshiftN DTCWT and MPCA in Laplacian Pyramid Domain. *Appl. Sci.* **2022**, *12*, 9495. <https://doi.org/10.3390/app12199495>

Academic Editors: Giovanni Dimauro, Rosalia Maglietta and Vito Renò

Received: 24 July 2022

Accepted: 2 September 2022

Published: 22 September 2022

Publisher's Note: MDPI stays neutral with regard to jurisdictional claims in published maps and institutional affiliations.



Copyright: © 2022 by the authors. Licensee MDPI, Basel, Switzerland. This article is an open access article distributed under the terms and conditions of the Creative Commons Attribution (CC BY) license (<https://creativecommons.org/licenses/by/4.0/>).

1. Introduction

The statistical analysis of images is restricted due to the depth of focus while sensing different images. The main problem is that the focus is not equally concentrated on objects which exist in an image [1]. A feasible solution to overcome the above problem is composite imaging. Composite imaging is one of the techniques used in Multi-focus Image Fusion (MIF), which combines multiple numbers of images with the concentration of different focus levels related to the same scene [2]. The spatial and transform domain methods are applicable in MIF [3]. Transform base methods are also called multiresolution algorithms. The main principle of transform domain algorithms is to maintain perceptual vision with accurate information in a multiresolution representation. Various studies indicate that several multiresolution methods have been developed, such as discrete wavelet transform (DWT), stationary wavelet transform (SWT), double density discrete wavelet transform

(DDDWT), etc. [4–15]. Lack of spatial orientation selectivity is the main issue with pyramid-based approaches, which causes blocking effects in the fused image. These pitfalls can be avoided by using DWT. However, DWT has issues with directionality, shift invariance, and aliasing. Primary factors influencing the quality of fused images are shift-invariance and directional selectivity. Traditional wavelet-based fusion techniques generate ringing artifacts into the fused images, which restricts the use of DWT for image fusion.

The DTCWT [16,17], one of the most accurate ones, overcomes the DWT's limitations in shift invariance and directional sensitivity. The directional selectivity and near-shift invariance of DTCWT allow it to properly represent features in the fused image. Developing filters in DTCWT is a little more challenging since bi-orthogonal, and phase limitations must be met. The qshift DTCWT is a technique for simplifying filter design in DTCWT that produces superior fusion outcomes. The qshift DTCWT has succeeded as a multi-resolution transform intended for image fusion because it can capture directional and shift invariant characteristics.

The objective of the proposed approach is to create a high-quality fused image that is smoother, has improved visuality, and is free of distortions and noise. Users can easily perceive details in these images. The majority of MIF algorithms have an inadequate spatial resolution, which causes blurring. On fused images, the qshiftN DTCWT approach has a significant impact. This technique effectively enhances the resolution of fused images and yields high-quality results. The LP [18–20], and MPCA [19] methods also do better in terms of lowering additive noise, reducing distortion, and maintaining edges and other crucial values such as image sectors with higher contrast. As shown by the visual, and quantitative results, the proposed method gets rid of these problems and produces better quality measurement results. Furthermore, the proposed formulation performs well in MIF.

Several approaches for MIF were proposed in the past decades. For example, in the Nonsubsampled Contourlet Transform (NSCT) domain, Chinmaya Panigrahy et al. proposed an effective image fusion model using an enhanced adaptive pulse coupled neural network (PCNN). The proposed methodology has utilized the subbands of the source images obtained by the NSCT algorithm in the image fusion process. The adaptive linking strength is estimated using a new fractal dimension-based focus measure FDFM algorithm [21]. A review of region-based fusion techniques was presented by Bikash Meher et al. based on the classification of region-based fusion approaches. For the comparison of the mentioned existing approaches, fusion objective assessment indicators are emphasized [22]. Lin He, and colleagues proposed a MIF approach for improving imaging systems. The cascade forest was incorporated into MIF to estimate the influence of fusion rules [23]. Samet Aymaz et al. proposed a unique MIF approach based on a super-resolution hybrid method [24].

In the DWT domain, Zeyu Wang et al. [25] proposed a novel MIF approach that uses a convolutional neural network (CNN) algorithm to combine the benefits of both spatial and transforms domain approaches. Instead of using image blocks or source images, CNN is employed to amplify features and build various decision maps for different frequency subbands. The additional benefit of the CNN approach is to utilize the adaptive fusion rule in the fusion process. Amin-Naji et al. [26] derived two important feature metrics the energy of Laplacian and the variance of Laplacian. The idea of the proposed work is to evaluate the correlation coefficient between the source blocks and the artificial blurred blocks in the discrete cosine transform (DCT) domain using the focus metrics. A new approach for MIF is proposed by Samet Aymaz et al. [27]. A super-resolution method is concerned with contrast enhancement, SWT with the combination of Discrete Meyer filter for decomposition. The further final image is attained by implementing a new fusion rule with a gradient-based approach. Wavelet transformations are introduced by Jinjiang Li et al. [28] to extract high and low-frequency coefficients. In addition to this deep convolution, neural networks are implemented to generate a high-quality fused image by direct mapping in between learning high-frequency and low-frequency of source images [29]. Mansour Nejati et al. [30] presented a new focus metric based on the surface

area of regions using the encircled method. This measure's ability to discriminate blurred regions in the fusion method is demonstrated. Bingzhe Wei et al. [31] a novel fusion method that applies CNN to assist sparse representation (SR) is proposed for the purpose of gaining a fused image with more precise and abundant information. The computational complexity of this fusion method is impressively reduced. Chenglang Zhang [32] proposed a novel MIF approach based on multiscale transform (MST) and convolution sparse representation (CSR) to address the inherent defects of both the MST and SR-based fusion methods. The proposed approach is put up against the approaches discussed in the literature [21–28,30].

The following are the essential contributions of this work:

- (i) A hybrid method (i.e., qshiftN DTCWT and LP) with MPCA is introduced for the fusion of multifocus images;
- (ii) The method helps combine multiple source images to develop a fused image having better image quality with good directionality, a high degree of shift-invariance, achieving better visual quality, and retaining more information than the source images;
- (iii) Using the MPCA method, the amount of redundant data is decreased, and the most significant components of the source images are extracted;
- (iv) Extend the depth-of-field (DOF) of the advanced imaging system;
- (v) An analyzing procedure has been done both quantitatively and qualitatively;
- (vi) Proposed approach performance has improved compared with the state-of-the-art techniques developed in recent years.

The rest of the paper is organized as follows: Section 2 explains the proposed fusion methodology as well as the fusion methods implemented. Section 3 presents the results of the experimentation. Section 4 concludes with conclusions.

2. The Proposed Fusion Approach

This paper proposes a hybrid approach with MPCA to overcome other algorithms' blurring and spatial distortions. An algorithm is a novel approach in MIF because this hybrid technique with MPCA gives good performance compared to other algorithms in recent years. In the proposed method, the fusion procedure is performed individually on row and column images, which are then averaged to eliminate any noise or distortion generated by the fusion process. The noise elimination process is explained in Section 2.1. Then, the source images are decomposed into LF components and HF components using LP. It provides information on the sharp contrast changes to which the human visual system is principally sensitive. The LP method is explained in Section 2.2. Then, qshiftN DTCWT is used to fuse low and high-frequency components to produce a fused image with good directionality and a high degree of shift-invariance. The qshiftN DTCWT method is explained in detail in Section 2.3. After fusing the low and high-frequency components, IDTCWT is applied to reconstruct the fused low and high-frequency components. In the proposed method, MPCA is used to improve the efficiency of the hybrid approach (i.e., qshiftN DTCWT and LP) to reduce the redundant data and extract the essential components of the fused image (i.e., all-in-focus image). Also, MPCA emphasizes elements that have the most significant impact and are robust to noise. So, the MPCA reduces the blurring and spatial distortions; thus, the fused image has more detailed clarity, clear edges, and better visual and machine perception. The MPCA method is explained in Section 2.4. Finally, the fused image is formed and available for comparison. Various objective quality metrics are calculated to assess the proposed method's quality. These measures are described in Sections 2.6 and 2.7, respectively. Figure 1 depicts the proposed technique's flow diagram, detailed in Section 2.5.

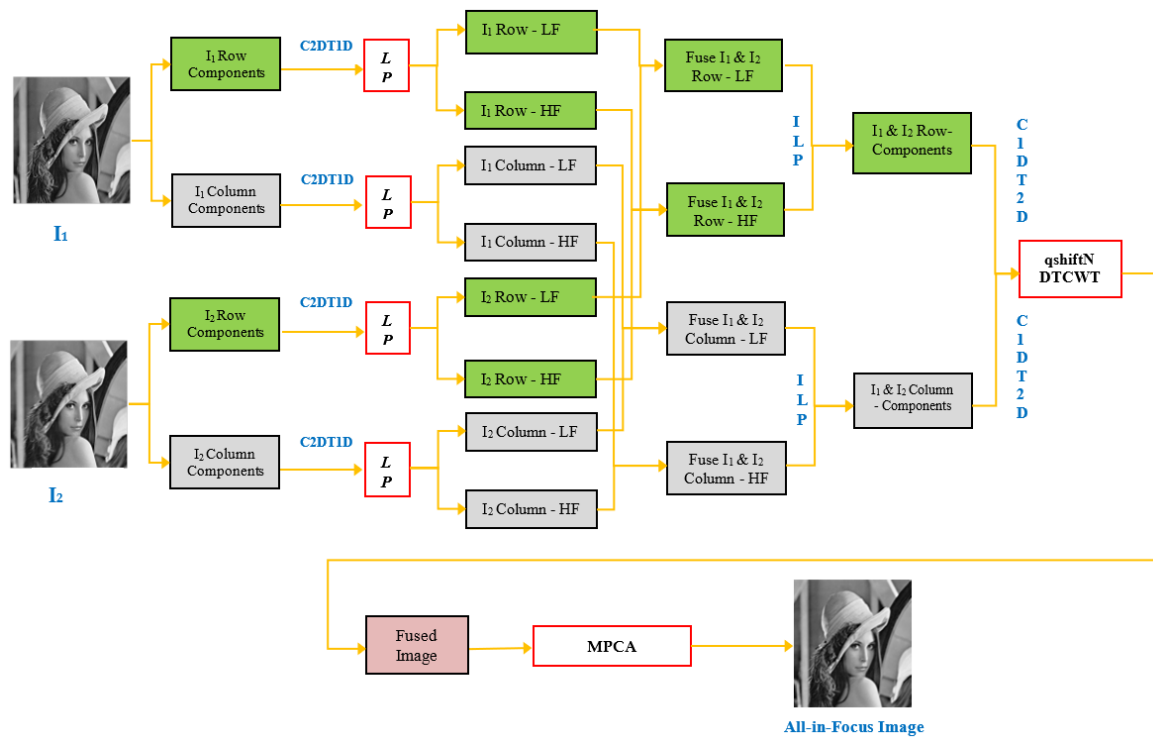


Figure 1. The flow diagram of the proposed qshiftN DTCWT-LP and MPCA-based image fusion algorithm.

2.1. Noise Elimination Process

The image $g(x, y)$ of size $M \times N$ is separated into rows, and the rows are concatenated to generate a 1-D vector data $g(x)$ of size MN [18]. It is shown in Algorithm 1.

Algorithm 1 Converting a two-dimensional array to a one-dimensional array

Input: Two-Dimensional Image (I), No. of Rows (M), and No. of Columns (N)

Output: One-Dimensional Vector Data (I)

Steps:

Begin

$$I(2 : 2 : END, :) = I(2 : 2 : END, END : -1 : 1)$$

$$I = RESHAPE(I', 1, M * N)$$

End

By inverting the technique mentioned in Algorithm 2, the 2-D image could be restored from the 1-D vector data.

Algorithm 2 Converting a one-dimensional array to a two-dimensional array

Input: One-Dimensional Vector Data (I), No. of Rows (M), and No. of Columns (N)

Output: Two-Dimensional Image (I)

Steps:

Begin

$$I = RESHAPE(I, M, N)'$$

$$I(2 : 2 : END, :) = I(2 : 2 : END, END : -1 : 1)$$

End

Likewise, the size image $g(x, y)$ is separated into columns and these columns are concatenated to generate a 1D vector data with $g(x)$ a size of MN . The operation is $I = C2DT1D(I', M, N)$.

2.2. Laplacian Pyramid (LP)

The Laplacian pyramid [18–20] reveals the strong contrast modifications to which the human visual system is most highly sensitive. It can localize in both the spatial and frequency domains. LP is used to extract the most relevant elements of the fused image. LP also sets a premium on elements that have the most effective and are resistant to noise. As a result, the LP minimizes blurring and spatial distortions. The technique for constructing and reconstructing a Laplacian pyramid is shown below. On vector data, the image reduction method is performed by taking the DCT and applying the inverse of the DCT (IDCT) to the first half of the coefficients. The function that reduces IR is used to conduct level-to-level image reduction.

Reduction Function (Image):

Image Reduction (IR) using DCT:

$$n = \text{length}(\text{Image}) \quad (1)$$

$$Y = \text{DCT}(\text{Image}, n) \quad (2)$$

$$\text{Image.LF} = \text{IDCT}(Y(1 : n/2)) \quad (3)$$

$$\text{Image.HF} = \text{Image} - \text{IDCT}(Y(1 : n/2), n) \quad (4)$$

Expand Image (IE) using DCT:

$$n = \text{length}(\text{Image.HF}) \quad (5)$$

$$\text{Image} = \text{DCT}(\text{Image.LF}) \quad (6)$$

$$\text{Image} = \text{IDCT}(\text{Image}, n) + \text{Image.HF} \quad (7)$$

Pyramid Construction:

$$X = \text{IR}(X) \quad (8)$$

$$I_k = x - \text{IE}(X) \quad (9)$$

Each image to be fused is formed into a pyramid using Equations (8) and (9). The constructed stages of the Laplacian pyramid are denoted by I_1 in the first image and I_2 in the second image. The following is the image fusion rule:

for $i = 1 : J$

$$\text{IMAGE1}\{i\} = \text{reduce}(I_1) \quad (10)$$

$$\text{IMAGE2}\{i\} = \text{reduce}(I_2) \quad (11)$$

$$\text{image1} = \text{IMAGE1}\{i\}.L \quad (12)$$

$$\text{image2} = \text{IMAGE2}\{i\}.L \quad (13)$$

end

$$\text{At } J^{\text{th}} \text{ level, } \text{IMAGEf}.L = 0.5 * (\text{IMAGE1}\{J\}.L + \text{IMAGE2}\{J\}.L) \quad (14)$$

for $J - 1$ to 1 levels

$$D = (\text{abs}(\text{IMAGE1}\{i\}.H) - \text{abs}(\text{IMAGE2}\{i\}.H)) >= 0 \quad (15)$$

$$\text{IMAGEf}.H = D.*\text{IMAGE}\{i\}.H + (\sim D).*\text{IMAGE2}\{i\}.H \quad (16)$$

$$\text{IMAGEf}.L = \text{expand}(\text{IMAGEf}) \quad (17)$$

end

$$\text{FusedImage} = \text{convert_1D_to_2D}(\text{IMAGEf}.L, m, n) \quad (18)$$

2.3. *qshiftN Dual-Tree Complex Wavelet Transform*

Highly sampled DWT exhibits change invariance issues in 1-D and directional sensitivity in N-D. The DTCWT approach is shift-invariant, economical, and directionally selective. The DTCWT [33,34] is an improved wavelet transformation that generates actual and imagined transformational coefficients. The DTCWT uses two 2-channel FIR filter banks. Output is the actual component of one filter bank (Tree A), whereas yield is the imaginary component (Tree B).

For a d -dimensional object, the DTCWT uses two significantly sampled filter banks with a 2^d redundancy. The three stages of a 1-D DTCWT filter bank are shown in Figure 2. While DWT-fused images have broken borders, DTCWT-fused images are soft and unbroken. When compared to DWT, which only delivers constrained directions in $(0^\circ, 45^\circ, 90^\circ)$, DTCWT produces 6 subbands in each of the three $(\pm 15^\circ, \pm 45^\circ, \pm 75^\circ)$, both real and imaginary, which improves transformational correctness and preserves more detailed features.

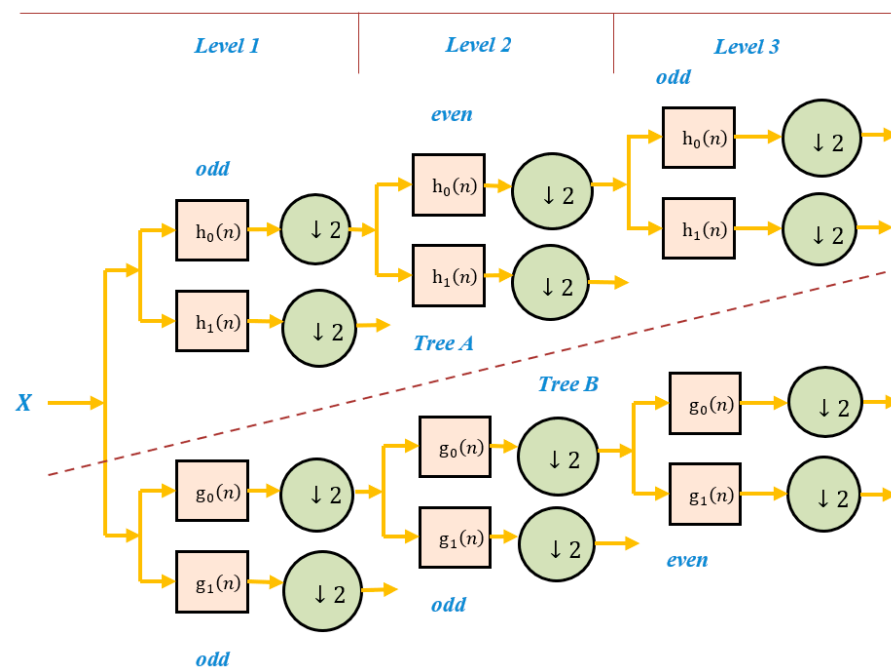


Figure 2. DTCWT bank filter's structure.

The odd/even filter approach proposed by DTCWT, however, has a number of drawbacks:

1. There is no clear symmetry in the sub-sampling structure;
2. The frequency reactions of the two trees vary slightly;
3. Otherwise, since both terms denote linearity, the filter sets must be biorthogonal rather than orthogonal. It demonstrates that energy efficiency does not apply to signals and fields.

Each of them is reduced and solved using the DTCWT *qshiftN* as illustrated in Figure 3, with all filters above level 1 much shorter. It is possible to achieve a sample gap above levels 1, and 1/2 during a test period by using delayed filters of 1/4 and 3/4 rather than the DTCWT original's 0 and 1/2. An asymmetric equal-length filter and the time it takes will be used to accomplish this.

Wavelet orthonormality can be perfectly transformed because of the asymmetry. When it comes to reverse filters, Tree-A filters are used, but Tree-B filters are used for both reverse and reconstruction filters because they are all part of the same orthonormal array. All trees have the same response in terms of their natural frequency. Individual effects are symmetrical around their midpoints, but the total complex impulses are asymmetric. Asymmetrical extension continues to work on the frame's edges because of this.

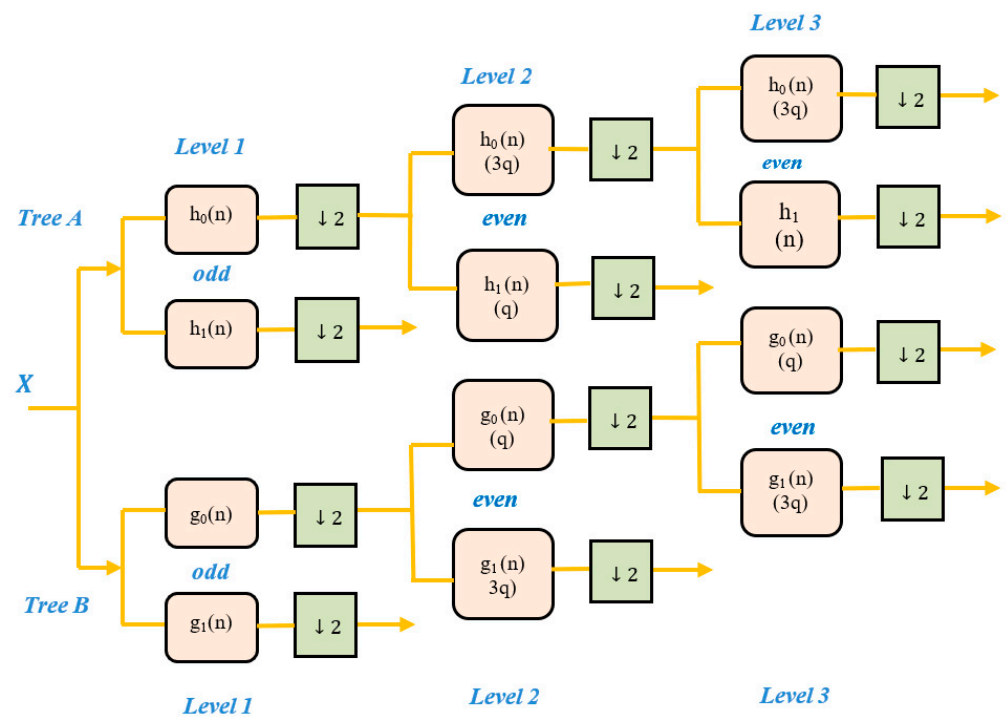


Figure 3. The qshiftN DTCWT filter’s structure.

2.4. Modified Principal Component Analysis (MPCA)

MPCA is used to turn uncorrelated variables into correlated variables. This method is useful for analyzing data and determining the optimal features for data collection. The first principal component represents data with the greatest variance. The others are just as much of what is left. The data is well represented by the first principal component, which also illustrates the direction of maximum variation. In this paper, the MPCA approach is used to determine the best-represented value of each subband of source images after implementing the LP-based qshiftN DTCWT method. These values are then multiplied by matched source image subbands. MPCA’s goal is to transfer data from the original space to the Eigen space. By saving the components with the largest eigenvector, the variance of the data is enhanced, and the covariance is lowered.

Specifically, this method removes redundant data from source images and extracts the most significant components. Furthermore, MPCA prioritizes components with the greatest impact and resistance to noise. As a result, the MPCA decreases blurring and spatial distortions. The steps of the MPCA algorithm are as follows:

1. Create a vector from the data
2. Determine the covariance matrix of the given vector
(i.e., $cov([im1(:)])$)
3. Calculate the eigenvalues and eigenvectors of the covariance matrices
(i.e., $[V, D] = eig(C)$)
4. Choose the first principal component in the order of the eigenvectors
(i.e., $[max, ind] = sort(diag(D), 'descend')$)
 $a = V(:, ind(1))./sum(V(:, ind(1)))$
5. Finally, to get the features extracted image (i.e., $F_E_image = a(1) * im1$)

2.5. Flow Diagram of Proposed Approach

The flow diagram of the complete fusion algorithm is depicted in Figure 1, which comprises two processes: LP-based qshiftN-DTCWT image fusion and MPCA. LP is used for decomposition, DTCWT is used for image fusion, and MPCA is used for feature extraction, as shown in Algorithm 3.

Algorithm 3 LP-based qshiftN DTCWT image fusion process and LP

Input: Multi-focus images.

Output: All-in-Focus Image

Steps:

- (i) Take the multi-focus images from the source and load them;
 - (ii) To use the image fusion technique, two multi-focus images ($I1$ and $I2$) are used as source images. Row ($I1$ and $I2$) and column ($I1$ and $I2$) pixels are used to divide raw images;
 - (iii) Multi-focus image row and column pixels are converted from a Two-Dimensional image to a One-Dimensional array of data;
 - (iv) Laplacian pyramid is used to divide the resulting 1-D array data ($I1$) into minimum (row and column frequencies) and maximum (row and column frequencies) frequency elements. The $I2$ image is split into low (row and column frequencies) and high (row and column frequencies) frequency components in the same way;
 - (v) To produce low and high-frequency row components, the primary fusion procedure is performed on row elements (both low and high-frequency elements) of $I1$ and $I2$. Similarly, to generate minimum and maximum frequency column elements, this fusion technique is used to process the column elements;
 - (vi) To produce row and column elements, the fused row, and column frequency components are filtered utilizing the Inverse laplacian pyramid algorithm;
 - (vii) The row and column elements of the 1-D array data are converted into a 2-D image;
 - (viii) Using qshiftN DTCWT, a final fused image is created from the filtered row and column frequency elements;
 - (ix) Apply MPCA on a fused image by qshiftN DTCWT-LP;
 - (x) Featured extracted image i.e., all-in-Focus image.
-

2.6. Evaluation of the Proposed Method's Effectiveness

In this section, the performance of the proposed technique is compared to that of state-of-the-art techniques in two ways: subjectively and objectively. Subjective assessment is a qualitative evaluation of how good the fused image looks. On the other hand, objective assessment, also called quantitative evaluation, is done by correlating the values of many image fusion efficiency metrics. Mathematical modeling is the basis for this quantitative method, which is called "objective analysis." It looks at how similar the fused image is to the images that were used to make it. With and without a reference image, there are two ways to do quantitative analysis [11,21,35–51].

This paper compared fourteen metrics: SF , $E(F)$, SD , AG , $RMSE$, CC , $Q^{AB/F}$, $L^{AB/F}$, $SSIM$, Q_E , $N^{AB/F}$, $PSNR$, and these measures are explained in Section 2.7.

2.7. Measuring Performance with Objective Quality Metrics

$E(F)$ (Entropy): It assists in the extraction of meaningful information from an image. A high level of entropy indicates that the image carries more than information.

AG (Average-Gradient): It determines the sharpness and clarity of an image. It shows that when the value of AG is high, the fused image has more clarity and sharpness.

CC (Correlation-Coefficient): It assesses the similarity of the all-in-focus image to the input images. For a better fusion process, a higher CC value is desired.

$SSIM$ (Structural-Similarity-Index-Measure): It assists in the correlation of two images' local patterns of the brightness of pixels. $SSIM$ has a range of -1 to 1 in its value.

Q_E (Edge-dependent Fusion Quality): This metric considers features of the human visual system, such as edge detail sensitivity. A greater Q_E value suggests that the fusion process is more efficient.

SD (Standard Deviation): The higher the *SD* number, the noisier the final image. Noise is more likely to impact images with lower contrast.

SF (Spatial-Frequency): It is used to determine the total intensity of activeness. When the all-in-focus image activity level is really high, it indicates that *SF* is quite high.

RMSE (Root Mean Square Error): It is useful for calculating the variations per pixel caused by image fusion methods. The value of *RMSE* rises as the similarity decreases.

PSNR (Peak-Signal-to-Noise-Ratio): It compares the similarity of the produced fused image and the reference image to determine image quality. The better the *PSNR* number, the better the fusion results.

In addition, objective image fusion effectiveness assessment via gradient information [11] is examined. Assessing total fusion performance (TFP), fusion loss (FL), and fusion artifacts (FA), provides a complete analysis of fusion performance. The process intended for calculating these metrics is detailed in [11], and their symbolic representation is presented below:

$Q^{AB/F}$ denotes the total amount of data transferred from the source images to the all-in-focus image. The method's performance is good if $Q^{AB/F}$ values are higher; $L^{AB/F}$, Total loss of information. The method's performance is good if $L^{AB/F}$ values are lower, and $N^{AB/F}$. Due to the fusion process, noise or artifacts have been added to the fused image. The method's performance is good if $N^{AB/F}$ values are lower.

3. Experimental Results

This paper proposes a qshiftN DTCWT and MPCA in laplacian pyramid domain. Quality measures include *SD*, $Q^{AB/F}$, $E(F)$, *AG*, *SF*, *CC*, *SSIM*, Q_E , Q_W , *FMI*, $L^{AB/F}$, $N^{AB/F}$, *RMSE*, and *PSNR* were employed to assess the algorithm's quality. These metrics are used to contrast the proposed technique to the methods that have been published in the past. The resemblance and robustness of the fused images against distortions are measured using these criteria. Source images for comparison are commonly used in MIF. Experiments are also carried out on many images from various areas and datasets [52]. In these images, the proposed approach yields good results. However, these images are not included in the paper because the techniques that are contrasted with the proposed approach do not produce outcomes for these images. Desk, balloon, book, clock, flower, lab, leaf, leopard, flowerpot, Pepsi, wine, and craft images are used to compare methodologies in the literature with [21–28,30]. In addition, the outcomes of the proposed technique for certain tried source images were presented. The images are of various sizes and qualities. The proposed method is applicable to any multi-focus images, not only those presented in this work.

3.1. The Outcomes of Some of the Images That Were Tried

Several grayscale images are used to implement the proposed technique. To analyze these images, *SF*, $Q^{AB/F}$, Q_E , *AG*, $E(F)$, *SSIM*, *SD*, and *CC* were used. It analyses a variety of images. Figures 4–8 show the visual outcomes for the images of a balloon, a leopard, a calendar, a bottle of wine, and a craft, respectively. Table 1 displays the results of the proposed method for specific trailing images. The subjective measurement outcomes (i.e., *RMSE* and *PSNR*) of certain trailing multi-focus images are depicted in Table 1. Table 2 compares the proposed technique to methods in the literature that use subjective criteria. Measurements for the stated image are not measured for the mentioned article, as shown by the letter X. In contrast, the proposed technique to methods in the literature, the flowerpot, clock, Pepsi, cameraman, desk, book, lab, and flower images are used. The best outcomes are shown in bold. The robustness of the proposed technique to deformation is measured using these criteria. The outcomes suggest that the proposed technique performs well in subjective measurements.

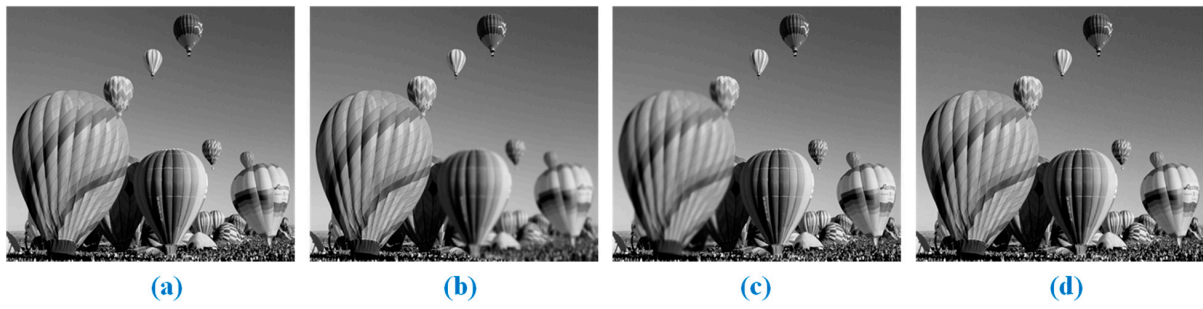


Figure 4. (Balloon): (a) Original Image; (b,c) Multi-focus input images; (d) Proposed fusion.

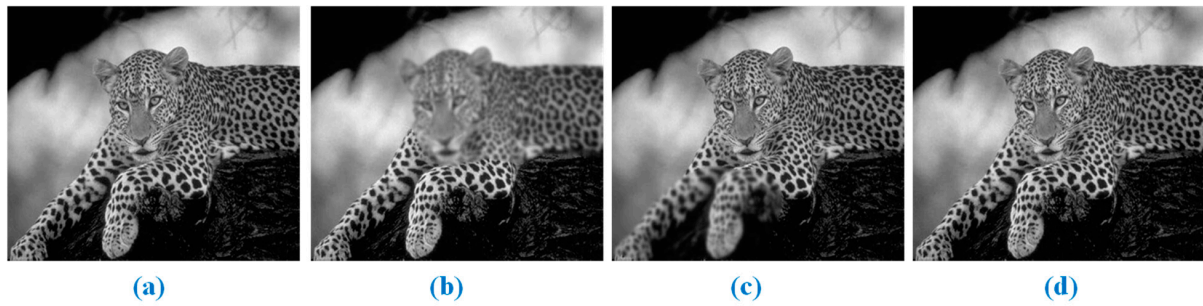


Figure 5. (Leopard): (a) Original Image; (b,c) Multi-focus input images; (d) Proposed fusion.

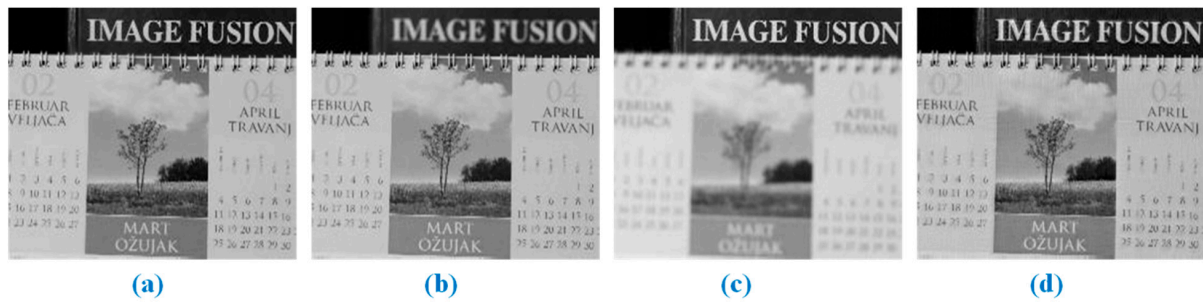


Figure 6. (Calendar): (a) original image; (b,c) multi-focus input images; and (d) proposed fusion.

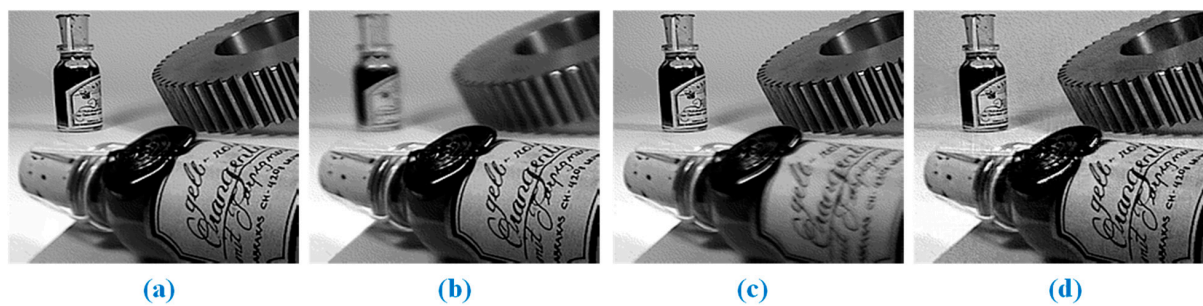


Figure 7. (Wine): (a) Original Image; (b,c) Multi-focus input images; (d) Proposed fusion.

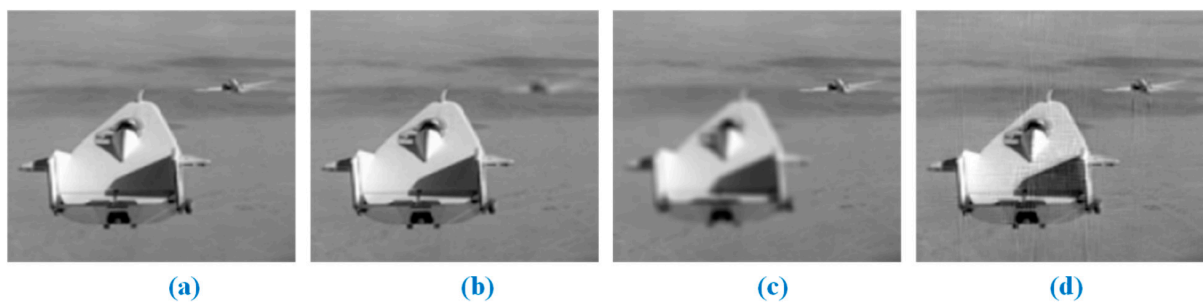


Figure 8. (Craft): (a) original image; (b,c) multi-focus input images; and (d) proposed fusion.

Table 1. For certain trailed images, the outcomes of the proposed method.

Input Images	RMSE	PSNR	SD	SF	SSIM	E(F)	$Q^{AB/F}$	AG	CC	Q_E
Book	9.8416	38.2341	60.9389	25.0770	0.9085	7.4362	0.9376	13.0210	0.9892	0.9165
Clock	4.4502	41.6810	51.1783	9.2224	0.9576	7.4180	0.9835	6.1301	0.9816	0.8997
Flower	5.1433	41.0524	39.6769	22.3338	0.9753	7.2315	0.9915	14.7327	0.9669	0.9058
Lab	4.0437	42.0970	47.7172	13.4651	0.9639	7.1517	0.9908	7.5892	0.9776	0.9196
Leaf	11.9434	37.3935	46.7165	32.0547	0.7898	7.4633	0.9582	26.9816	0.9219	0.8305
Flowerpot	5.3262	40.9006	53.5593	24.1377	0.9638	7.5211	0.9908	14.4599	0.9750	0.9131
Pepsi	2.7651	43.7477	45.6264	14.2884	0.9730	7.1431	0.9955	8.5574	0.9819	0.9439
Balloon	1.7621	45.7045	48.5287	21.0675	0.9904	7.4875	0.9990	10.2507	0.9840	0.9534
Leopard	2.1108	44.9204	66.0408	20.0953	0.9909	7.4777	0.9988	13.6941	0.9893	0.9491
Wine	10.0433	38.1460	72.2601	51.7072	0.8938	7.6116	0.9784	35.6507	0.9492	0.8705
Craft	4.6617	41.4794	31.8556	13.4799	0.9374	6.5221	0.9823	7.5230	0.9660	0.8807
Desk	4.8765	41.2838	47.6417	16.1341	0.9448	7.3882	0.9871	9.4234	0.9624	0.9216

Table 2. For some images, the comparisons with approaches in the literature.

IF-Methods	Image Metrics	Lab	Desk	Clock	Book	Camerman	Flower	Pepsi	Flowerpot
C. Rama Mohan et al. [53]	RMSE	X	7.44	5.85	X	9.06	X	3.83	7.43
	PSNR	X	39.45	40.50	X	38.59	X	42.34	39.46
Li et al. [54]	RMSE	4.65	X	X	X	X	7.84	X	X
	PSNR	X	X	X	X	X	X	X	X
Moushmi et al. [55]	RMSE	X	X	4.51	7.04	X	X	X	X
	PSNR	X	X	X	X	X	X	X	X
Proposed Method	RMSE	5.14	9.84	4.45	4.044	4.88	5.33	2.77	5.33
	PSNR	41.05	38.23	41.68	42.09	41.28	40.90	43.75	40.90

3.2. Comparison of Multi-Focus Image (i.e., Clock)

The evaluation of the first multi-focus image is the clock, illustrated in Figure 9. Figure 9a represents the original image. Figure 9b,c illustrate left-focused and right-focused images, respectively. The term “left-focused image” refers to the fact that the image’s left side is focused while the right side is not. A “right-focused image” is one in which the image’s right side is focused, but its left side is not. Figure 9d shows that the all-in-focus image is created when the approach is implemented. $E(F)$, AG , CC , $Q^{AB/F}$, $SSIM$, Q_E , SF , and QW are calculated to assess the proposed methodology performance. Finally, the performance of the proposed approach is compared to that of other methods previously published in the literature. The results of the comparison are shown in Tables 3–8 of the report. The letter X indicates that metrics are not calculated for the article depicted in the image. According to the literature [21,22,24,27,28,30], the proposed method is more successful than those approaches, and the best outcomes of methods are indicated in bold.

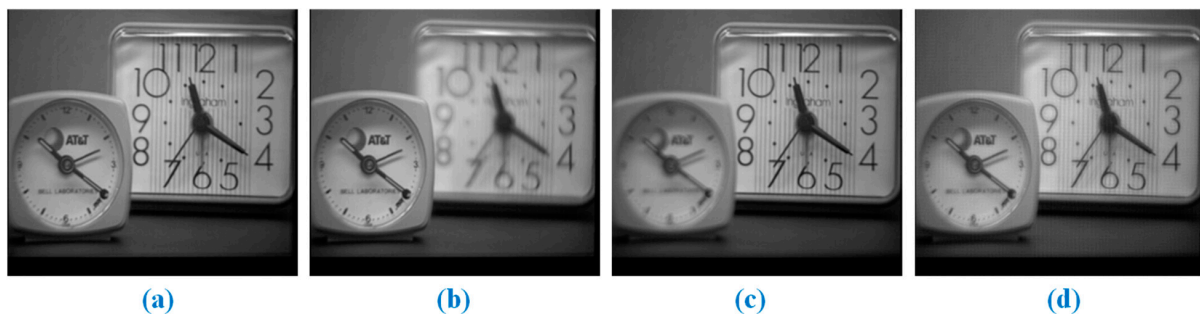
**Figure 9.** (Clock): (a) original image; (b,c) multi-focus input images; and (d) proposed fusion.

Table 3. The outcomes for the clock image and comparisons with existing techniques in the literature ([21]).

Evaluation Metric	GFDF	NSC-PCNN	LG-MW	IM	DCT-CV	QT	GF	MST-SR	DSIFT	CSR	SSDI	CNN	BF	BRW-TS	PA-DCPCNN	Proposed Method
$E(F)$	7.077	7.304	7.067	7.170	6.992	6.986	7.249	7.321	7.014	7.318	7.123	7.128	7.008	7.078	7.385	7.418
Q_E	0.853	0.803	0.840	0.848	0.841	0.848	0.852	0.850	0.850	0.850	0.853	0.855	0.848	0.854	0.854	0.899
AG_F	5.802	5.411	5.860	5.746	5.810	5.866	5.841	5.879	5.857	5.382	5.848	5.751	5.774	5.757	6.072	6.130
$SSIM$	0.895	0.900	0.894	0.900	0.894	0.894	0.897	0.903	0.894	0.897	0.896	0.896	0.894	0.896	0.903	0.958
$Q^{AB/F}$	0.892	0.873	0.880	0.850	0.869	0.880	0.895	0.893	0.894	0.889	0.893	0.891	0.881	0.890	0.897	0.984
CC	0.978	0.981	0.978	0.978	0.978	0.978	0.980	0.981	0.978	0.979	0.979	0.979	0.978	0.979	0.981	0.982

Table 4. The outcomes for the clock image and comparisons with existing techniques in the literature ([22]).

Evaluation Metric	QWT Normalized Cut	RF-SSIM	NSCT & Focus Area Detection	BEMD	Surface Area Based	RSSF	SR	Shearlet & GBVS	CS	LSWT	Proposed Method
$Q^{AB/F}$	0.744	0.429	0.750	0.483	0.74	0.703	0.753	0.717	0.426	0.725	0.984
SF	8.398	9.100	8.473	9.193	13.65	8.986	8.468	8.708	8.562	8.046	9.2224
Q_E	0.665	0.665	0.582	0.663	X	0.652	0.592	0.586	0.494	0.583	0.899
Q_w	0.843	0.852	0.834	0.834	X	0.821	0.781	0.736	0.776	0.763	0.9192
H	7.342	7.426	7.291	7.346	X	7.369	7.066	7.434	7.412	7.155	7.418

Table 5. The outcomes for the clock image and comparisons with existing techniques in the literature ([24]).

Evaluation Metric	Samet Aymaz et al. SR	Baohua et al.	Li et al.	Hua et al.	Zhang et al.	Samet Aymaz et al. without SR	Yin et al.	Proposed Method
$Q^{AB/F}$	0.9	0.7	0.68	0.73	0.71	0.78	0.71	0.984
AG	6.97	X	X	X	X	4.26	3.46	6.130

Table 6. The outcomes for the clock image and comparisons with existing techniques in the literature ([27]).

Methods	$Q^{AB/F}$
Nejati et al.	0.72
Samet Aymaz et al.—with SR-2	0.87
Du et al.	X
Jiang et al.	0.71
Samet Aymaz et al.—with SR-4	0.89
Li et al.	0.68
Chaudhary et al.	X
Amin-Naji et al.	X
Abdipour et al.	0.65
Hua et al.	0.73
He et al.	0.69
He et al.	X
Samet Aymaz et al.—with SR-3	0.88
Chen et al.	X
Aymaz et al.	0.9
Yin et al.	0.71
Zhang et al.	0.71
Yang et al.	0.74
Proposed Method	0.984

Table 7. The outcomes for the clock image and comparisons with existing techniques in the literature ([28]).

Evaluation Metric	PCNN	NSCT	DCNN	SR	DSIFT	MWG	NSCT-SR	GF	WDCNN	Proposed Method
AG	5.57	4.53	4.56	4.34	4.44	4.44	4.55	4.58	6.52	6.130
SSIM	0.65	0.54	0.65	0.53	0.58	0.60	0.53	0.61	0.69	0.958

Table 8. The outcomes for the clock image and comparisons with existing techniques in the literature ([30]).

Evaluation Metric	CBF	DCHWT	DCTVAR	GFF	IFM	MWGF	WSSM	SA-FC	Proposed Method
SF	12.87	12.28	13.52	13.43	13.29	13.42	13.6	13.65	9.2224
$Q^{AB/F}$	0.726	0.694	0.735	0.733	0.735	0.731	0.709	0.74	0.984

3.3. Comparison of Multi-Focus Image (i.e., Desk)

The evaluation of the second multi-focus image is the desk, illustrated in Figure 10. Figure 10a represents the original image. Figure 10b,c illustrates left-focused and right-focused images, respectively. The term “left-focused image” refers to the fact that the image’s left side is focused while the right side is not. An image with a right focus indicates that it has been focused on its right side only, while its left side has not been focused on. Figure 10d shows the process of creating the all-in-focus image after the method has been successfully implemented. The following parameters are computed to evaluate the proposed methodology performance: $E(F)$, AG, CC, $Q^{AB/F}$, SSIM, Q_E , FMI, SD, QW, $L^{AB/F}$, $N^{AB/F}$, and SF. Finally, the performance of the proposed approach is compared to that of other methods previously published in the literature. The results of the comparison are shown in Tables 9–15 of the report. The letter X indicates that metrics are not calculated for the article depicted in the image. According to the literature [21,23–27,30], the proposed method is more successful than those approaches, and the best outcomes of methods are indicated in bold.

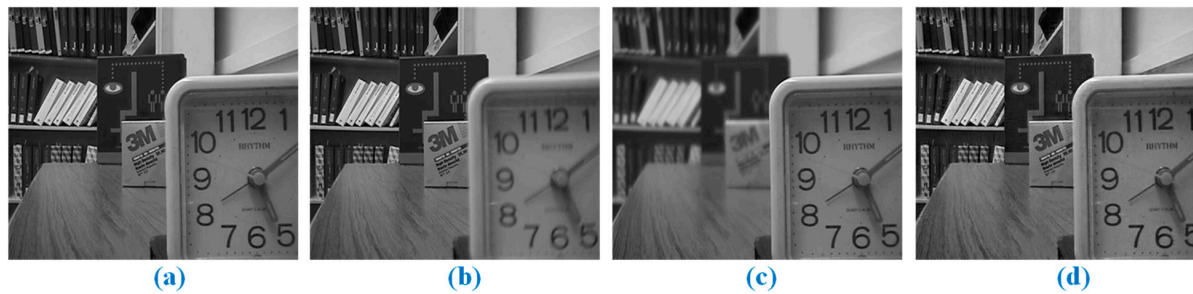


Figure 10. (Desk): (a) original image; (b,c) multi-focus input images; and (d) proposed fusion.

Table 9. The outcomes for the desk image and comparisons with existing techniques in the literature ([21]).

Evaluation Metric	PA-DCPCNN	NSC-PCNN	BRW-TS	LG-MW	GFDF	DCT-CV	IM	CNN	GF	BF	SSDI	QT	DSIFT	CSR	MST-SR	Proposed Method
$E(F)$	7.346	7.298	7.284	7.296	7.279	7.272	7.284	7.280	7.309	7.270	7.308	7.280	7.291	7.294	7.311	7.388
Q_E	0.867	0.849	0.865	0.864	0.864	0.829	0.848	0.863	0.866	0.834	0.865	0.864	0.863	0.863	0.869	0.922
$SSIM$	0.869	0.860	0.858	0.853	0.856	0.855	0.856	0.858	0.862	0.856	0.857	0.855	0.855	0.860	0.867	0.945
$Q^{AB/F}$	0.896	0.887	0.891	0.888	0.891	0.875	0.883	0.890	0.893	0.874	0.892	0.892	0.891	0.888	0.896	0.987
CC	0.964	0.964	0.961	0.960	0.961	0.960	0.961	0.961	0.962	0.960	0.961	0.960	0.960	0.961	0.964	0.962
AG	8.215	7.822	7.973	8.057	7.995	7.953	7.956	7.957	7.921	7.897	8.053	8.068	8.071	7.570	8.122	9.423

Table 10. The outcomes for the desk image and comparisons with existing techniques in the literature ([23]).

Evaluation Metric	CF	SR	CVT	CNN	NSCT	GFF	NSCT-SR	Proposed Method
SD	46.860	46.589	46.766	46.817	46.869	46.860	46.576	47.642
FMI	0.675	0.579	0.533	0.674	0.575	0.592	0.574	0.390
$Q^{AB/F}$	0.734	0.702	0.686	0.734	0.702	0.711	0.702	0.987

Table 11. The outcomes for the desk image and comparisons with existing techniques in the literature ([24]).

Evaluation Metric	Samet Aymaz et al. without SR	Baohua et al.	Zhang et al.	Hua et al.	Chen et al.	Samet Aymaz et al. SR	Proposed Method
AG	6.6	X	X	X	X	11.86	9.423
$Q^{AB/F}$	0.84	0.71	0.68	0.73	0.71	0.88	0.987

Table 12. The outcomes for the desk image and comparisons with existing techniques in the literature ([25]).

Evaluation Metric	DWT	LP	Curvelet	IMF	CNN	DS	DCTCV	MWGF	GFF	CNN-DWT	Proposed Method
Q_E	0.8896	0.8958	0.8974	0.8923	0.8982	0.8971	0.8878	0.8982	0.8973	0.8985	0.9216
Q_w	0.8655	0.8727	0.8779	0.8711	0.8775	0.8761	0.868	0.8757	0.8775	0.8782	0.9090

Table 13. The outcomes for the desk image and comparisons with existing techniques in the literature ([26]).

Methods	$Q^{AB/F}$	$L^{AB/F}$	$N^{AB/F}$
DCT + Average	0.5187	0.4782	0.0063
DCT + Variance	0.7165	0.2612	0.0478
DCT + Contrast	0.6212	0.2554	0.3629
DWT	0.6302	0.2552	0.3362
SIDWT	0.6694	0.2764	0.1564
DCHWT	0.6529	0.314	0.0789
DCT + SML	0.6774	0.3074	0.0324
DCT + Eng_Corr	0.7288	0.253	0.0391
DCT + SF	0.7213	0.26	0.0415
DCT + VOL	0.7285	0.2519	0.0421
DCT + EOL	0.728	0.2522	0.0425
DCT + AC_Max	0.6763	0.291	0.0696
DCT + Corr	0.7246	0.2541	0.0456
Proposed Method	0.9871	0.0071	0.0117

Table 14. The outcomes for the desk image and comparisons with existing techniques in the literature ([27]).

Methods	$Q^{AB/F}$
Samet Aymaz et al.—with SR-4	0.89
Jiang et al.	0.72
Hua et al.	0.73
Li et al.	X
Samet Aymaz et al.—with SR-2	0.87
Nejati et al.	0.73
Yang et al.	0.73
Abdipour et al.	X
Zhang et al.	0.68
Yin et al.	X
Chaudhary et al.	0.71
He et al.	X
He et al.	X
Du et al.	X
Aymaz et al.	0.88
Amin-Naji et al.	X
Samet Aymaz et al.—with SR-3	0.88
Chen et al.	0.71
Proposed Method	0.9871

Table 15. The outcomes for the desk image and comparisons with existing techniques in the literature ([30]).

Evaluation Metric	SA-FC	CBF	DCHWT	MWGF	DCTVAR	GFF	IFM	WSSM	Proposed Method
SF	15.54	14.92	13.83	15.45	15.39	15.42	15.42	15.47	16.1341
$Q^{AB/F}$	0.739	0.699	0.655	0.728	0.732	0.726	0.725	0.702	0.9871

3.4. Comparison of Multi-Focus Image (i.e., Book)

The evaluation of the third multi-focus image is the book, illustrated in Figure 11. Figure 11a represents the original image. Figure 11b,c illustrate left-focused and right-focused images, respectively. The term “left-focused image” refers to the fact that the image’s left side is focused, while the right side is not. The right side of the image is focused while the left is not. Figure 11d shows the process of creating the all-in-focus image after the method has been successfully implemented. The following parameters are computed to evaluate the proposed methodology performance: $E(F)$, AG , CC , $Q^{AB/F}$, $SSIM$, Q_E , QW , $L^{AB/F}$, $N^{AB/F}$, and SF . Finally, the performance of the proposed approach is compared to that of other methods previously published in the literature. The results of the comparison are shown in Tables 16–21 of the report. The letter X indicates that metrics are not calculated for the article depicted in the image. According to the literature [21,24–27,30], the proposed method is more successful than those approaches, and the best outcomes of methods are indicated in bold.

3.5. Comparison of Multi-Focus Image (i.e., Flower)

The evaluation of the fourth multi-focus image is the flower, illustrated in Figure 12. Figure 12a represents the original image. Figure 12b,c illustrates left-focused and right-focused images, respectively. The term “left-focused image” refers to the fact that the image’s left side is focused while the right side is not. A right-focused image is one in which the image’s right side is focused, but its left side is not. Figure 12d shows that the all-in-focus image is created when the approach is implemented. $E(F)$, AG_F , CC , $Q^{AB/F}$, $SSIM$, and Q_E are calculated to assess the proposed methodology performance. Finally, the performance of the proposed approach is compared to that of other methods previously published in the literature. The comparison results are shown in Tables 22 and 23 of the report. The letter X indicates that metrics are not calculated for the article depicted in the image. According to the literature [21,24], the proposed method is more successful than those approaches, and the best outcomes of methods are indicated in bold.

3.6. Comparison of Multi-Focus Image (i.e., Lab)

The evaluation of the fifth multi-focus image is the lab, which is illustrated in Figure 13. Figure 13a represents the original image. Figure 13b,c illustrate left-focused and right-focused images, respectively. The term “left-focused image” refers to the fact that the image’s left side is focused while the right side is not. An image with a right focus indicates that it has been focused on its right side only, while its left side has not been focused on. Figure 13d shows the process of creating the all-in-focus image after the method has been successfully implemented. The following parameters are computed to evaluate the proposed methodology performance: $E(F)$, AG , CC , $Q^{AB/F}$, $SSIM$, Q_E , QW , and SF . Finally, the performance of the proposed approach is compared to that of other methods previously published in the literature. The results of the comparison are shown in Tables 24–29 of the report. The letter X indicates that metrics are not calculated for the article depicted in the image. According to the literature [21,24,25,27,28,30], the proposed method is more successful than those approaches, and the best outcomes of methods are indicated in bold.

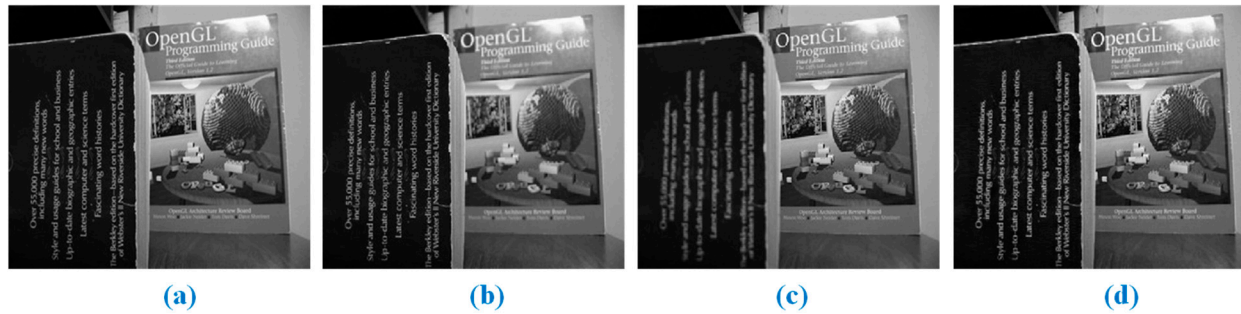


Figure 11. (Book): (a) original Image; (b,c) multi-focus input images; and (d) proposed fusion.

Table 16. The outcomes for the book image and comparisons with existing techniques in the literature ([21]).

Evaluation Metric	PA-DCPCNN	NSC-PCNN	BRW-TS	LG-MW	GFDF	DCT-CV	IM	CNN	GF	MST-SR	BF	QT	CSR	DSIFT	SSDI	Proposed Method
SSIM	0.954	0.952	0.952	0.951	0.952	0.952	0.951	0.952	0.952	0.954	0.952	0.952	0.953	0.952	0.952	0.909
$Q^{AB/F}$	0.915	0.906	0.907	0.905	0.907	0.905	0.905	0.908	0.908	0.908	0.906	0.905	0.908	0.906	0.907	0.938
CC	0.983	0.982	0.982	0.982	0.982	0.982	0.982	0.982	0.982	0.982	0.982	0.982	0.982	0.982	0.982	0.989
AG	13.706	13.377	13.412	13.436	13.409	13.418	13.354	13.373	13.373	13.518	13.411	13.428	12.645	13.457	13.438	13.021
Q_E	0.884	0.879	0.882	0.881	0.882	0.879	0.876	0.883	0.883	0.883	0.881	0.880	0.883	0.881	0.882	0.917
$E(F)$	7.296	7.295	7.271	7.270	7.268	7.270	7.266	7.270	7.265	7.275	7.269	7.271	7.249	7.273	7.271	7.436

Table 17. The outcomes for the book image and comparisons with existing techniques in the literature ([24]).

Evaluation Metric	Samet Aymaz et al. without SR	Chen et al.	Li et al.	Zhang et al.	Liu et al.	Samet Aymaz et al. SR	Hua et al.	Proposed Method
AG	10.83	X	X	X	9.36	13.9	X	13.021
$Q^{AB/F}$	0.81	0.71	0.71	0.72	0.79	0.92	0.73	0.938

Table 18. The outcomes for the book image and comparisons with existing techniques in the literature ([25]).

Evaluation Metric	DWT	LP	Curvelet	IMF	CNN	DS	DCTCV	MWGF	GFF	CNN-DWT	Proposed Method
Q_E	0.8942	0.8962	0.8999	0.8911	0.9007	0.9002	0.8827	0.9	0.901	0.8993	0.917
Q_w	0.8932	0.8969	0.9024	0.8957	0.9029	0.9017	0.8897	0.9014	0.9026	0.9031	0.9363

Table 19. The outcomes for the book image and comparisons with existing techniques in the literature ([26]).

Methods	$L^{AB/F}$	$Q^{AB/F}$	$N^{AB/F}$
DCT + Average	0.5002	0.4985	0.0025
DCT + Variance	0.266	0.721	0.0277
DCT + Contrast	0.2384	0.647	0.3736
DWT	0.2294	0.6621	0.3569
DCT + Eng_Corr	0.2622	0.7284	0.0202
DCHWT	0.3014	0.6684	0.0705
SIDWT	0.2637	0.6932	0.1279
DCT + EOL	0.262	0.7283	0.0206
DCT + SML	0.2928	0.696	0.0241
DCT + SF	0.2757	0.7151	0.0197
DCT + VOL	0.2619	0.7284	0.0207
DCT + Corr	0.2622	0.7281	0.0207
DCT + AC_Max	0.2781	0.7081	0.0294
Proposed Method	0.0422	0.938	0.0403

Table 20. The outcomes for the book image and comparisons with existing techniques in the literature ([27]).

Methods	$Q^{AB/F}$
Chen et al.	0.71
Abdipour et al.	0.73
Samet Aymaz et al.—with SR-4	0.93
Hua et al.	0.73
Jiang et al.	0.73
Zhang et al.	X
Chaudhary et al.	X
Nejati et al.	0.73
Amin-Naji et al.	X
Samet Aymaz et al.—with SR-3	0.91
Yang et al.	0.76
He et al.	X
He et al.	0.76
Yin et al.	X
Aymaz et al.	0.92
Samet Aymaz et al.—with SR-2	0.9
Du et al.	0.72
Li et al.	0.71
Proposed Method	0.938

Table 21. The outcomes for the book image and comparisons with existing techniques in the literature ([30]).

Evaluation Metric	CBF	DCHWT	DCTVAR	GFF	IFM	MWGF	WSSM	SA-FC	Proposed Method
$Q^{AB/F}$	0.728	0.688	0.731	0.732	0.729	0.731	0.728	0.734	0.938
SF	28.08	25.11	30.08	29.98	30.38	29.91	27.49	30.1	25.0770

**Figure 12.** (Flower): (a) original image; (b,c) multi-focus input images; and (d) proposed fusion.

Table 22. The outcomes for the flower image and comparisons with existing techniques in the literature ([21]).

Evaluation Metric	PA-DCPCNN	NSC-PCNN	BRW-TS	LG-MW	GFDF	DCT-CV	SSDI	CNN	IM	GF	QT	CSR	DSIFT	MST-SR	BF	Proposed Method
Q_E	0.862	0.850	0.855	0.853	0.856	0.850	0.855	0.856	0.852	0.856	0.854	0.857	0.854	0.860	0.851	0.906
AG	14.316	12.813	14.114	14.182	14.102	14.126	14.141	14.053	14.115	14.083	14.207	13.348	14.217	14.148	13.969	14.733
SSIM	0.948	0.950	0.941	0.940	0.941	0.940	0.941	0.939	0.941	0.941	0.940	0.942	0.940	0.947	0.940	0.975
$Q^{AB/F}$	0.887	0.885	0.876	0.874	0.877	0.872	0.876	0.878	0.875	0.878	0.874	0.878	0.874	0.878	0.871	0.992
CC	0.969	0.969	0.962	0.961	0.962	0.961	0.962	0.962	0.961	0.963	0.961	0.963	0.961	0.967	0.961	0.967
$E(F)$	7.221	7.152	7.181	7.181	7.181	7.182	7.180	7.180	7.181	7.185	7.182	7.168	7.182	7.191	7.179	7.232

Table 23. The outcomes for the flower image and comparisons with existing techniques in the literature ([24]).

Evaluation Metric	Liu et al.	Samet Aymaz et al. without SR	Samet Aymaz et al. SR	Proposed Method
AG	9.22	9.47	18.08	14.733
$Q^{AB/F}$	0.71	0.79	0.85	0.992



Figure 13. (Lab): (a) original image; (b,c) multi-focus input images; and (d) proposed fusion.

Table 24. The outcomes for the lab image and comparisons with existing techniques in the literature ([21]).

Evaluation Metric	PA-DCPCNN	NSC-PCNN	BRW-TS	LG-MW	CNN	DCT-CV	IM	GF	CSR	QT	DSIFT	MST-SR	SSDI	BF	GFDF	Proposed Method
SSIM	0.912	0.909	0.907	0.905	0.907	0.906	0.904	0.910	0.909	0.906	0.906	0.911	0.907	0.907	0.907	0.964
AG	6.647	6.336	6.482	6.514	6.457	6.466	6.484	6.425	6.126	6.504	6.534	6.594	6.539	6.456	6.479	7.589
$Q^{AB/F}$	0.900	0.893	0.896	0.892	0.896	0.893	0.893	0.898	0.896	0.896	0.896	0.900	0.897	0.895	0.896	0.991
$E(F)$	7.118	6.992	7.075	7.037	7.022	6.982	7.056	7.060	7.043	7.039	7.074	7.110	7.096	6.989	7.032	7.152
CC	0.979	0.979	0.977	0.977	0.977	0.977	0.977	0.978	0.978	0.977	0.977	0.979	0.977	0.977	0.977	0.978
Q_E	0.868	0.850	0.865	0.862	0.865	0.863	0.861	0.867	0.864	0.865	0.864	0.868	0.865	0.863	0.865	0.919

Table 25. The outcomes for the lab image and comparisons with existing techniques in the literature ([24]).

Evaluation Metric	Chen et al.	Hua et al.	Zhang et al.	Li et al.	Samet Aymaz et al. without SR	Samet Aymaz et al. SR	Proposed Method
AG	X	X	X	X	4.8	7.81	7.589
$Q^{AB/F}$	0.73	0.74	0.73	0.73	0.84	0.89	0.991

Table 26. The outcomes for the lab image and comparisons with existing techniques in the literature ([25]).

Evaluation Metric	DWT	LP	Curvelet	IMF	CNN	DS	DCTCV	MWGF	GFF	CNN-DWT	Proposed Method
Q_E	0.8787	0.8855	0.8871	0.8849	0.8885	0.8883	0.8806	0.8884	0.8892	0.8875	0.919
Q_w	0.8748	0.8807	0.8849	0.8825	0.8844	0.8831	0.8799	0.8832	0.8829	0.885	0.9147

Table 27. The outcomes for the lab image and comparisons with existing techniques in the literature ([27]).

Methods	$Q^{AB/F}$
Zhang et al.	0.73
Abdipour et al.	0.75
Jiang et al.	0.73
Hua et al.	0.74
Amin-Naji et al.	0.75
He et al.	0.73
Chaudhary et al.	0.68
Samet Aymaz et al.—with SR-2	0.88
Yang et al.	X
Aymaz et al.	0.89
Du et al.	0.75
Yin et al.	X
Samet Aymaz et al.—with SR-4	0.9
He et al.	X
Nejati et al.	0.74
Chen et al.	0.73
Samet Aymaz et al.—with SR-3	0.89
Li et al.	0.73
Proposed Method	0.991

Table 28. The outcomes for the lab image and comparisons with existing techniques in the literature ([28]).

Evaluation Metric	NSCT	GF	NSCT-SR	MWG	DSIFT	DCNN	PCNN	SR	WDCNN	Proposed Method
AG	9.35	9.56	9.54	9.50	9.45	9.89	9.70	9.46	10.35	7.59
$SSIM$	0.48	0.51	0.50	0.51	0.50	0.50	0.51	0.48	0.51	0.96

Table 29. The outcomes for the lab image and comparisons with existing techniques in the literature ([30]).

Evaluation Metric	WSSM	CBF	DCHWT	SA-FC	DCTVAR	GFF	IFM	MWGF	Proposed Method
SF	11.94	12.24	11.2	12.97	12.96	12.86	12.94	13.01	13.4651
$Q^{AB/F}$	0.707	0.712	0.663	0.748	0.746	0.738	0.738	0.737	0.991

3.7. Comparison of Multi-Focus Image (i.e., Leaf)

The evaluation of the sixth multi-focus image is the leaf, which is illustrated in Figure 14. Figure 14a represents the original image. Figure 14b,c illustrates left-focused and right-focused images, respectively. The term “left-focused image” refers to the fact that the image’s left side is focused, while the right side is not. The right side of the image is focused while the left is not. Figure 14d shows the process of creating the all-in-focus image after the method has been successfully implemented. The following parameters are computed to evaluate the proposed methodology performance: $E(F)$, AG , CC , $Q^{AB/F}$, $SSIM$, Q_E , and SF . Finally, the performance of the proposed approach is compared to that of other methods previously published in the literature. The results of the comparison are shown in Tables 30–32 of the report. The letter X indicates that metrics are not calculated for the article depicted in the image. According to the literature [21,24,30], the proposed method is more successful than those approaches, and the best outcomes of methods are indicated in bold.

3.8. Comparison of Multi-Focus Image (i.e., Pepsi)

The evaluation of the seventh multi-focus image is the pepsi, which is illustrated in Figure 15. Figure 15a represents the original image. Figure 15b,c illustrate left-focused and right-focused images, respectively. The term “left-focused image” refers to the fact that the image’s left side is focused while the right side is not. A right-focused image is one in which the image’s right side is focused, but its left side is not. Figure 15d shows that the all-in-focus image is created when the approach is implemented. AG , $Q^{AB/F}$, Q_E , SF , and QW are calculated to assess the proposed methodology performance. Finally, the performance of the proposed approach is compared to that of other methods previously published in the literature. The results of the comparison are shown in Tables 33–36 of the report. The letter X indicates that metrics are not calculated for the article depicted in the image. According to the literature [24,25,27,30], the proposed method is more successful than those approaches, and the best outcomes of methods are indicated in bold.

3.9. Comparison of Multi-Focus Image (i.e., Flowerpot)

The evaluation of the eighth multi-focus image is the flowerpot, which is illustrated in Figure 16. Figure 16a represents the original image. Figure 16b,c illustrate left-focused and right-focused images, respectively. The term “left-focused image” refers to the fact that the image’s left side is focused while the right side is not. An image with a right focus indicates that it has been focused on its right side only, while its left side has not been focused on. Figure 16d shows the process of creating the all-in-focus image after the method has been successfully implemented. The following parameters are computed to evaluate the proposed methodology performance: Q_E , and QW . Finally, the performance of the proposed approach is compared to that of other methods previously published in the literature. The results of the comparison are shown in Table 37 of the report. The letter X indicates that metrics are not calculated for the article depicted in the image. According to the literature [25], the proposed method is more successful than those approaches, and the best outcomes of methods are indicated in bold.

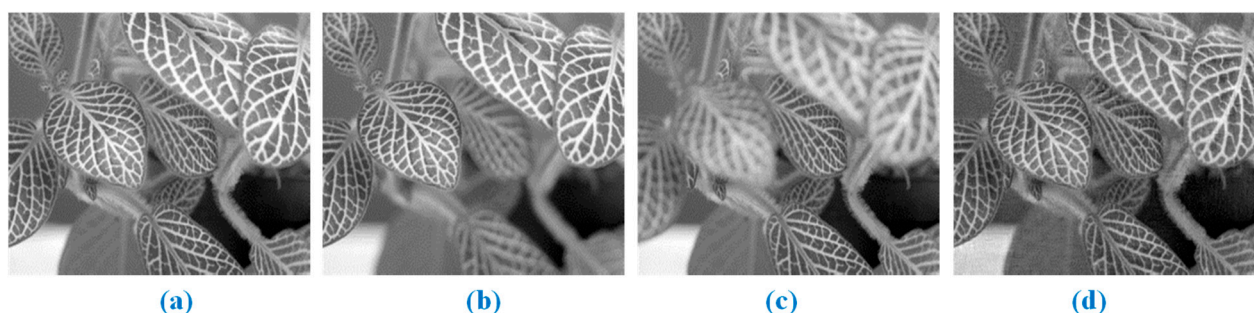


Figure 14. (Leaf): (a) original image; (b,c) multi-focus input images; and (d) proposed fusion.

Table 30. The outcomes for the leaf image and comparisons with existing techniques in the literature ([21]).

Evaluation Metric	NSC-PCNN	GFDF	LG-MW	DCT-CV	IM	GF	QT	BRW-TS	DSIFT	MST-SR	SSDI	PA-DCPCNN	CSR	BF	CNN	Proposed Method
$Q^{AB/F}$	0.871	0.880	0.873	0.839	0.880	0.881	0.877	0.880	0.877	0.883	0.880	0.887	0.877	0.875	0.880	0.958
Q_E	0.797	0.822	0.814	0.783	0.818	0.822	0.820	0.822	0.821	0.824	0.823	0.812	0.820	0.810	0.819	0.831
AG	18.318	18.713	18.923	18.103	18.878	18.635	19.038	18.756	19.054	19.031	18.929	19.176	18.179	18.775	18.449	26.982
SSIM	0.742	0.742	0.736	0.729	0.740	0.745	0.735	0.743	0.736	0.746	0.740	0.759	0.741	0.739	0.746	0.789
$E(F)$	7.313	7.339	7.344	7.268	7.343	7.347	7.343	7.340	7.345	7.375	7.343	7.406	7.334	7.341	7.334	7.463
CC	0.926	0.927	0.925	0.904	0.926	0.929	0.925	0.926	0.925	0.932	0.926	0.937	0.927	0.925	0.928	0.922

Table 31. The outcomes for the leaf image and comparisons with existing techniques in the literature ([24]).

Evaluation Metric	Yin et al.	Samet Aymaz et al. SR	Baohua et al.	Zhang et al.	Samet Aymaz et al. Without SR	Proposed Method
$Q^{AB/F}$	0.73	0.88	0.73	0.69	0.75	0.958
AG	10.88	24.18	X	X	11.97	26.982

Table 32. The outcomes for the leaf image and comparisons with existing techniques in the literature ([30]).

Evaluation Metric	CBF	DCHWT	DCTVAR	GFF	IFM	MWGF	WSSM	SA-FC	Proposed Method
SF	13.88	11.97	14.02	14.24	14.3	11.57	9.48	14.34	32.0547
$Q^{AB/F}$	0.721	0.689	0.751	0.751	0.746	0.608	0.735	0.763	0.958

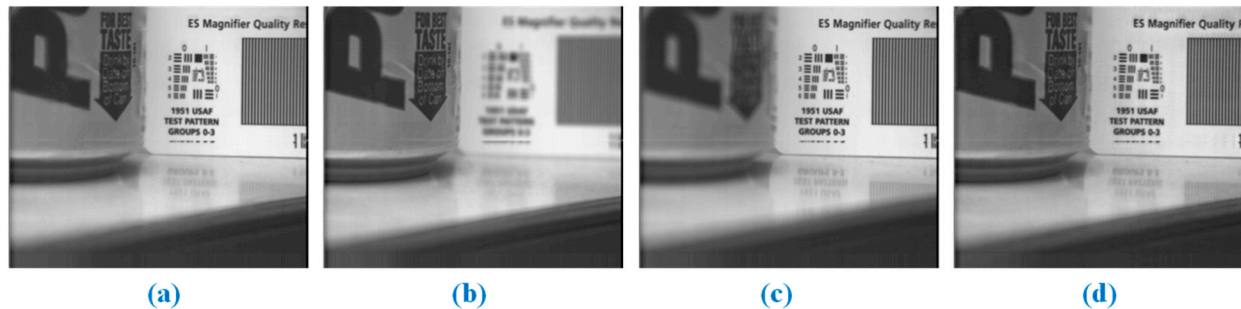


Figure 15. (Pepsi): (a) original image; (b,c) multi-focus input images; and (d) proposed fusion.

Table 33. The outcomes for the Pepsi image and comparisons with existing techniques in the literature ([24]).

Evaluation Metric	Hua et al.	Li et al.	Yin et al.	Zhang et al.	Baohua et al.	Samet Aymaz et al. without SR	Chen et al.	Samet Aymaz et al. SR	Proposed Method
AG	X	X	4.01	X	X	6	X	15.06	8.5574
$Q^{AB/F}$	0.76	0.76	0.78	0.78	0.75	0.81	0.75	0.93	0.9955

Table 34. The outcomes for the pepsi image and comparisons with existing techniques in the literature ([25]).

Evaluation Metric	DWT	LP	Curvelet	IMF	CNN	DS	DCTCV	MWGF	GFF	CNN-DWT	Proposed Method
Q_E	0.9154	0.9186	0.9216	0.9025	0.9223	0.9208	0.9185	0.9211	0.9232	0.9237	0.9439
Q_w	0.9118	0.915	0.9154	0.9095	0.9144	0.9132	0.9117	0.9132	0.9179	0.9184	0.9381

Table 35. The outcomes for the pepsi image and comparisons with existing techniques in the literature ([27]).

Methods	$Q^{AB/F}$
He et al.	0.78
Aymaz et al.	0.93
Yang et al.	X
Jiang et al.	0.78
Hua et al.	0.76
Li et al.	0.76
Zhang et al.	0.78
Chaudhary et al.	0.76
Nejati et al.	0.78
Amin-Naji et al.	X
Du et al.	X
Yin et al.	0.78
Chen et al.	0.75
He et al.	0.78
Abdipour et al.	0.79
Samet Aymaz et al.—with SR-2	0.91
Samet Aymaz et al.—with SR-3	0.92
Samet Aymaz et al.—with SR-4	0.93
Proposed Method	0.99

Table 36. The outcomes for the Pepsi image and comparisons with existing techniques in the literature ([30]).

Evaluation Metric	CBF	DCHWT	DCTVAR	GFF	IFM	MWGF	WSSM	SA-FC	Proposed Method
$Q^{AB/F}$	0.769	0.753	0.785	0.778	0.771	0.777	0.729	0.786	0.9955
SF	13.5	12.81	13.81	13.72	13.96	13.73	13.96	13.99	14.2884



Figure 16. (Flowerpot): (a) original image; (b,c) multi-focus input images; and (d) proposed fusion.

Table 37. The outcomes for the flowerpot image and comparisons with existing techniques in the literature ([25]).

Evaluation Metric	DWT	LP	Curvelet	IMF	CNN	DS	DCTCV	MWGF	GFF	CNN-DWT	Proposed Method
Q_E	0.8603	0.8687	0.8699	0.8679	0.8722	0.87	0.8692	0.8699	0.8723	0.8748	0.9131
Q_w	0.907	0.9147	0.925	0.9217	0.925	0.9233	0.9233	0.9215	0.925	0.9281	0.9223

3.10. Analysis of a Few More Image Pairs

A single strategy will never produce the ideal subjective and objective results for all image pairs. Because of this, eight multi-focus image pairings (shown in Figure 17) are used in the next experiment to demonstrate the average performance of various techniques, which is demonstrated in the following experiment. In the case of the image pairs in Figure 17, the proposed method produced fused images depicted in Figure 18. As shown in Figure 18, the results of the proposed approach fusion are satisfactory for all of the image pairs tested. For the image pairs in Figure 17, the average objective assessment of several methodologies is shown in Table 38. The results of the comparison are presented in Table 38. Comparing the proposed method to approaches described in the literature [21], the proposed method is more successful, and the best outcomes of the various methods are highlighted in bold.

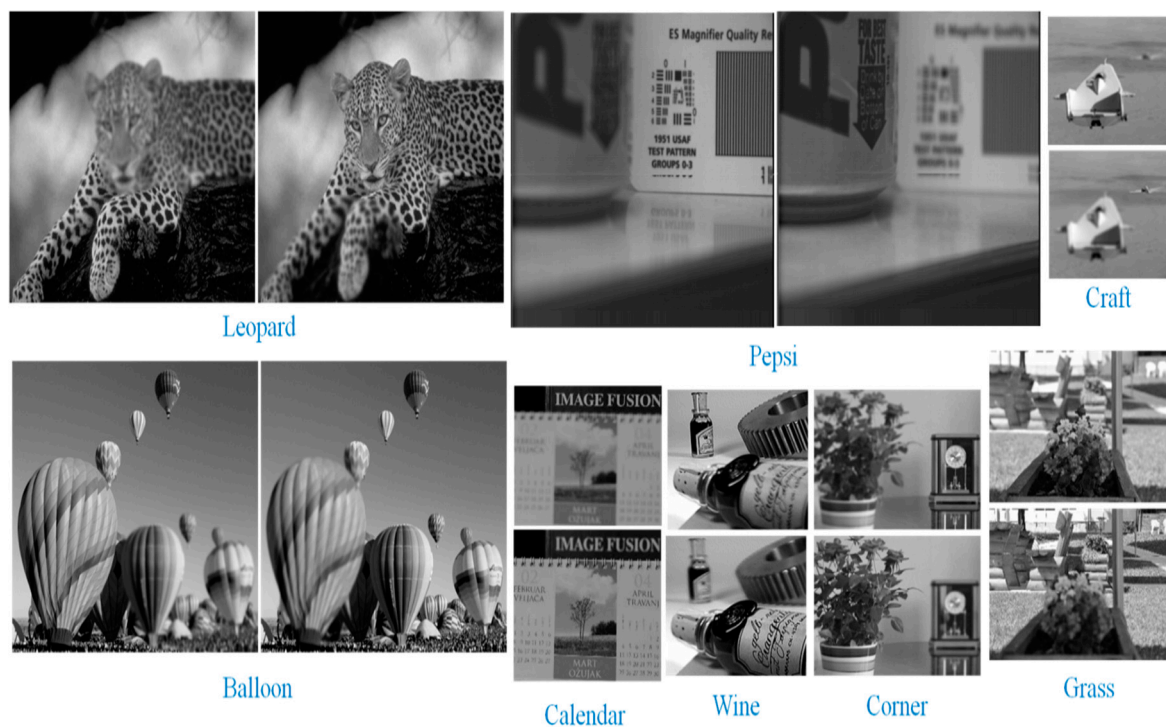
**Figure 17.** A few pairs of multi-focus images.



Figure 18. The multi-focus image sets in Figure 16 represent the fusion outcomes of the proposed technique.

Table 38. Comparative Analysis of quantitative measures (average value) ([21]).

Evaluation Metric	PA-DCPCNN	NSC-PCNN	CNN	LG-MW	GFDF	DCT-CV	IM	GF	BF	QT	DSIFT	MST-SR	SSDI	CSR	BRW-TS	Proposed Method
SSIM	0.872	0.860	0.859	0.856	0.859	0.854	0.859	0.864	0.857	0.856	0.856	0.868	0.859	0.861	0.859	0.958
$Q^{AB/F}$	0.898	0.881	0.886	0.882	0.885	0.877	0.883	0.887	0.883	0.883	0.883	0.891	0.885	0.883	0.885	0.991
CC	0.974	0.972	0.969	0.969	0.969	0.966	0.969	0.97	0.969	0.969	0.969	0.973	0.969	0.969	0.969	0.974
AG	15.120	14.419	14.629	14.848	14.699	14.723	14.686	14.524	14.744	14.843	14.846	14.835	14.749	13.849	14.703	15.023
Q_E	0.834	0.807	0.831	0.827	0.831	0.822	0.827	0.832	0.827	0.828	0.828	0.835	0.830	0.829	0.829	0.918
$E(F)$	7.277	7.30	7.226	7.229	7.227	7.212	7.227	7.234	7.224	7.225	7.225	7.257	7.228	7.232	7.226	7.292

4. Conclusions

The performance of the traditional wavelets-based fusion algorithms is to create ringing distortions in the fused image due to a lack of directional selectivity and shift-invariance. The proposed methodology utilizes the benefits of a hybrid method approach for the image fusion process. The hybrid method contains LP for decomposition, DTCWT for image fusion, and MPCA for feature extraction. The advantages of the proposed fused image are having better image quality and extracting relevant information from the source images with good directionality, a high degree of shift-invariance using hybrid approach with MPCA, due to this achieving better visual quality. Several pairs of multifocus images are used to assess the performance of the proposed method. Through the experiments conducted on standard test pairs of multifocus images, it was found that the proposed method has shown superior performance in most of the cases as compared to other methods in terms of quantitative parameters and in terms of visual quality, it has shown superior performance to that of other methods. Therefore, the proposed work is validated with many data sets to meet these goals by evaluating quantitative measures like $E(F)$, AG , SD , $SSIM$, $Q^{AB/F}$, etc. It is evident from the results that the proposed method produces better visual perception, better clarity, and less distortion. In this work, the proposed technique is used to fuse only grayscale images. Moreover, the application of the proposed method to other areas, such as medical image processing, infrared-visible image processing should be part of future exploration.

Author Contributions: Conceptualization, C.R.M., K.C., A.O.I. and N.Z.J.; Methodology, C.R.M., N.Z.J., R.K.R., K.S.S. and K.C.; Coding, C.R.M., A.A., A.O.I. and K.C.; Validation, N.Z.J., R.K.R., K.S.S., A.A. and C.R.M.; Investigation, R.K.R., K.C. and N.Z.J.; Resources, C.R.M., K.C. and A.O.I.; Writing—original draft preparation, C.R.M., K.C. and R.K.R.; Writing—review and editing, C.R.M., K.S.S., A.A. and K.C. All authors have read and agreed to the published version of the manuscript.

Funding: The authors extend their appreciation to the Deanship of Scientific Research at King Khalid University for funding this work through Large Groups. (Project under grant number (RGP2/111/43)).

Institutional Review Board Statement: Not applicable.

Informed Consent Statement: Not Applicable.

Data Availability Statement: Data can be available on request.

Acknowledgments: We acknowledge thanks to the Center for Smart Society 5.0 CSS5, Taylor's University, Malaysia.

Conflicts of Interest: The authors declare no conflict of interest.

References

1. Shah, P.; Merchant, S.N.; Desai, U.B. Multi-focus and multispectral image fusion based on pixel significance using multiresolution decomposition. *Signal Image Video Processing* **2013**, *7*, 95–109. [\[CrossRef\]](#)
2. Chai, Y.; Li, H.; Li, Z. Multi-focus image fusion scheme using focused region detection and multiresolution. *Opt. Commun.* **2011**, *284*, 4376–4389. [\[CrossRef\]](#)
3. Zhang, B.; Zhang, C.; Yuanyuan, L.; Jianshuai, W.; He, L. Multi-focus image fusion algorithm based on compound PCNN in Surfacelet domain. *Optik* **2014**, *125*, 296–300. [\[CrossRef\]](#)
4. Wahyuni, I.S.; Sabre, R. Wavelet Decomposition in Laplacian Pyramid for Image Fusion. *Int. J. Signal Processing Syst.* **2016**, *4*, 37–44. [\[CrossRef\]](#)
5. Petrovic, V.S.; Xydeas, C.S. Gradient-based multiresolution image fusion. *IEEE Trans. Image Processing* **2004**, *13*, 228–237. [\[CrossRef\]](#)
6. Wang, W.W.; Shui, P.; Song, G. Multi-focus Image Fusion in Wavelet Domain. Proceedings of the Second International Conference on Machine Learning and Cybernetics. *IEEE Comput. Soc.* **2003**, *5*, 2887–2890. [\[CrossRef\]](#)
7. Li, S.; Yang, B.; Hu, J. Performance comparison of different multi-resolution transforms for image fusion. *Inf. Fusion* **2011**, *12*, 74–84. [\[CrossRef\]](#)
8. Sharma, A.; Gulati, T. Change Detection from Remotely Sensed Images Based on Stationary Wavelet Transform. *Int. J. Electr. Comput. Eng.* **2017**, *7*, 3395–3401. [\[CrossRef\]](#)

9. Borwonwatanadelok, P.; Rattanapitak, W.; Udomhunsakul, S. Multi-focus Image Fusion Based on Stationary Wavelet Transform and Extended Spatial Frequency Measurement. In Proceedings of the 2009 International Conference on Electronic Computer Technology, Macau, China, 20–22 February 2009; pp. 77–81. [\[CrossRef\]](#)
10. Naidu, V. Image Fusion Technique using Multi-resolution Singular Value Decomposition. *Def. Sci. J.* **2011**, *61*, 479–484. [\[CrossRef\]](#)
11. Shreyamsha Kumar, B.K. Multi-focus and multispectral image fusion based on pixel significance using discrete cosine harmonic wavelet transform. *Signal Image Video Processing* **2013**, *7*, 1125–1143. [\[CrossRef\]](#)
12. Li, H.; Wei, S.; Chai, Y. Multi-focus image fusion scheme based on feature contrast in the lifting stationary wavelet domain. *EURASIP J. Adv. Signal Processing* **2012**, *39*. [\[CrossRef\]](#)
13. Yuelin, Z.; Xiaoqiang, L.; Wang, T. Visible and Infrared Image Fusion using the Lifting Wavelet. *Telecommun. Comput. Electron. Control.* **2013**, *11*, 6290–6295. [\[CrossRef\]](#)
14. Pujar, J.; Itkarkar, R.R. Image Fusion Using Double Density Discrete Wavelet Transform. *Int. J. Comput. Sci. Netw.* **2016**, *5*, 6–10.
15. Liu, J.; Yang, J.; Li, B. Multi-focus Image Fusion by SML in the Shearlet Subbands. *TELKOMNIKA Indones. J. Electr. Eng.* **2014**, *12*, 618–626. [\[CrossRef\]](#)
16. Selesnick, I.W.; Baraniuk, R.G.; Kingsbury, N.C. The dual-tree complex wavelet transform. *IEEE Signal Processing Mag.* **2005**, *22*, 123–151. [\[CrossRef\]](#)
17. Radha, N.; Ranga Babu, T. Performance evaluation of quarter shift dual tree complex wavelet transform based multi-focus image fusion using fusion rules. *Int. J. Electr. Comput. Eng.* **2019**, *9*, 2377–2385. [\[CrossRef\]](#)
18. Naidu, V.P.S. Novel Image Fusion Techniques using DCT. *Int. J. Comput. Sci. Bus. Inform.* **2013**, *5*, 1–18.
19. Rama Mohan, C.; Kiran, S.; Vasudeva; Ashok Kumar, A. Image Enhancement based on Fusion using 2D LPDCT and Modified PCA. *Int. J. Eng. Adv. Technol.* **2019**, *8*, 1482–1492.
20. Rama Mohan, C.; Ashok Kumar, A.; Kiran, S.; Vasudeva. An Enhancement Process for Gray-Scale Images Resulted from Image Fusion using Multiresolution and Laplacian Pyramid. *ICTACT J. Image Video Processing* **2021**, *11*, 2391–2399. [\[CrossRef\]](#)
21. Panigrahy, C.; Seal, A.; Mahato, N.K. Fractal dimension based parameter adaptive dual channel PCNN for multi-focus image fusion. *Opt. Lasers Eng.* **2020**, *133*, 106141–106163. [\[CrossRef\]](#)
22. Meher, B.; Agrawal, S.; Panda, R.; Abraham, A. A survey on region based image fusion methods. *Inf. Fusion* **2018**, *48*, 119–132. [\[CrossRef\]](#)
23. He, L.; Yang, X.; Lu, L.; Wu, W.; Ahmad, A.; Jeon, G. A novel multi-focus image fusion method for improving imaging systems by using cascade-forest model. *J. Image Video Proc.* **2020**, *2020*, 1–14. [\[CrossRef\]](#)
24. Aymaz, S.; Köse, C. A novel image decomposition-based hybrid technique with super-resolution method for multi-focus image fusion. *Inf. Fusion* **2019**, *45*, 113–127. [\[CrossRef\]](#)
25. Wang, Z.; Li, X.; Duan, H.; Zhang, X.; Wang, H. Multi-focus image fusion using convolutional neural networks in the discrete wavelet transform domain. *Multimed. Tools Appl.* **2019**, *78*, 34483–34512. [\[CrossRef\]](#)
26. Amin-Naji, M.; Aghagolzadeh, A. Multi-Focus Image Fusion in DCT Domain using Variance and Energy of Laplacian and Correlation Coefficient for Visual Sensor Networks. *J. AI Data Min.* **2018**, *6*, 233–250. [\[CrossRef\]](#)
27. Aymaz, S.; Köse, C.; Aymaz, Ş. Multi-focus image fusion for different datasets with super-resolution using gradient-based new fusion rule. *Multimed Tools Appl.* **2020**, *79*, 13311–13350. [\[CrossRef\]](#)
28. Li, J.; Yuan, G.; Fan, H. Multi-focus Image Fusion Using Wavelet-Domain-Based Deep CNN. *Comput. Intell. Neurosci.* **2019**, *2019*, 4179397. [\[CrossRef\]](#)
29. Chouhan, K.; Kumar, A.; Chakraverti, A.K.; Cholla, R.R. Human fall detection analysis with image recognition using convolutional neural network approach. In Proceedings of the International Conference on Trends in Computational and Cognitive Engineering, Lecture Notes in Network and Systems; Springer Nature: Singapore, 2022; Volume 376.
30. Nejati, M.; Samavi, S.; Karimi, N.; Soroushmehr, S.R.; Shirani, S.; Roosta, I.; Najarian, K. Surface area-based focus criterion for multi-focus image fusion. *Inf. Fusion* **2017**, *36*, 284–295. [\[CrossRef\]](#)
31. Wei, B.; Feng, X.; Wang, K.; Gao, B. The Multi-Focus-Image-Fusion Method Based on Convolutional Neural Network and Sparse Representation. *Entropy* **2021**, *23*, 827. [\[CrossRef\]](#)
32. Zhang, C. Multifocus image fusion using multiscale transform and convolutional sparse representation. *Int. J. Wavelets Multiresolution Inf. Processing* **2021**, *19*, 2050061. [\[CrossRef\]](#)
33. Yang, Y.; Tong, S.; Huang, S.; Lin, P. Dual-Tree Complex Wavelet Transform and Image Block Residual-Based Multi-Focus Image Fusion in Visual Sensor Networks. *Sensors* **2014**, *14*, 22408–22430. [\[CrossRef\]](#) [\[PubMed\]](#)
34. Xiao, Y.; Hong, Y.; Chen, X.; Chen, W. The Application of Dual-Tree Complex Wavelet Transform (DTCWT) Energy Entropy in Misalignment Fault Diagnosis of Doubly-Fed Wind Turbine (DFWT). *Entropy* **2017**, *19*, 587. [\[CrossRef\]](#)
35. Jagalingam, P.; Hegde, A.V. A Review of Quality Metrics for Fused Image. *Aquat. Procedia* **2015**, *4*, 133–142. [\[CrossRef\]](#)
36. Zafar, R.; Farid, M.S.; Khan, M.H. Multi-Focus Image Fusion: Algorithms, Evaluation, and a Library. *J. Imaging* **2020**, *6*, 60. [\[CrossRef\]](#) [\[PubMed\]](#)
37. Pistonesi, S.; Martinez, J.; Ojeda, S.M.; Vallejos, R. A Novel Quality Image Fusion Assessment Based on Maximum Codispersion. In *Progress in Pattern Recognition, Image Analysis, Computer Vision, and Applications*; CIARP 2015. Lecture Notes in Computer Science; Springer: Cham, Switzerland, 2015; Volume 9423. [\[CrossRef\]](#)
38. Sun, C.; Zhang, C.; Xiong, N. Infrared and Visible Image Fusion Techniques Based on Deep Learning: A Review. *Electronics* **2020**, *9*, 2162. [\[CrossRef\]](#)

39. Anisha, M.L.; Margret Anuncia, S. Enhanced Dictionary based Sparse Representation Fusion for Multi-temporal Remote Sensing Images. *Eur. J. Remote Sens.* **2016**, *49*, 317–336. [CrossRef]
40. Xydeas, C.S.; Petrovic, V. Objective image fusion performance measure. *Electron. Lett.* **2000**, *36*, 308–309. [CrossRef]
41. Liu, Z.; Blasch, E.; Xue, Z.; Zhao, J.; Laganieri, R.; Wu, W. Objective Assessment of Multiresolution Image Fusion Algorithms for Context Enhancement in Night Vision: A Comparative Study. *IEEE Trans. Pattern Anal. Mach. Intell.* **2012**, *34*, 94–109. [CrossRef]
42. Qu, G.; Zhang, D.; Yan, P. Information measure for performance of image fusion. *Electron. Lett.* **2002**, *38*, 313–315. [CrossRef]
43. Hossny, M.; Nahavandi, S.; Creighton, D. Comments on ‘Information measure for performance of image fusion’. *Electron. Lett.* **2008**, *44*, 1066–1067. [CrossRef]
44. Han, Y.; Cai, Y.; Cao, Y.; Xu, X. A New Image Fusion Performance Metric Based on Visual Information Fidelity. *Inf. Fusion* **2013**, *14*, 127–135. [CrossRef]
45. Wang, Q.; Shen, Y.; Jin, J. Performance evaluation of image fusion techniques. In *Image Fusion: Algorithms and Applications*; Stathaki, T., Ed.; Academic Press: Oxford, UK, 2008; pp. 469–492. [CrossRef]
46. Cvejic, N.; Canagarajah, C.; Bull, D. Image fusion metric based on mutual information and Tsallis entropy. *Electron. Lett.* **2006**, *42*, 626–627. [CrossRef]
47. Zheng, Y.; Essock, E.A.; Hansen, B.C.; Haun, A.M. A new metric based on extended spatial frequency and its application to DWT based fusion algorithms. *Inf. Fusion* **2007**, *8*, 177–192. [CrossRef]
48. Wang, Z.; Bovik, A.C.; Sheikh, H.R.; Simoncelli, E.P. Image quality assessment: From error visibility to structural similarity. *IEEE Trans. Image Processing* **2004**, *13*, 600–612. [CrossRef]
49. Yang, C.; Zhang, J.-Q.; Wang, X.-R.; Liu, X. A novel similarity based quality metric for image fusion. *Inf. Fusion* **2008**, *9*, 156–160. [CrossRef]
50. Chen, H.; Varshney, P.K. A human perception inspired quality metric for image fusion based on regional information. *Inf. Fusion* **2007**, *8*, 193–207. [CrossRef]
51. Chen, Y.; Blum, R.S. A new automated quality assessment algorithm for image fusion. *Image Vis. Comput.* **2009**, *27*, 1421–1432. [CrossRef]
52. Available online: <https://sites.google.com/view/durgaprasadbavirisetti/datasets> (accessed on 1 December 2021).
53. Rama Mohan, C.; Kiran, S.; Ashok Kumar, A. Advanced Multi-focus Image Fusion algorithm using FPDCT with Modified PCA. *Int. J. Innov. Technol. Explor. Eng.* **2019**, *9*, 175–184. [CrossRef]
54. Li, H.; Chai, Y.; Yin, H.; Liu, G. Multi-focus image fusion denoising scheme based on homogeneity similarity. *Opt. Commun.* **2012**, *285*, 91–100. [CrossRef]
55. Moushmi, S.; Sowmya, V.; Soman, K.P. Empirical wavelet transform for multi-focus image fusion. In *Proceedings of the International Conference on Soft Computing Systems, Advances in Intelligent Systems and Computing 2016*; Springer: Berlin/Heidelberg, Germany, 2018.